JOURNAL OF MATERIALS SCIENCE 30 (1995) 6179–6191

Interlaminar fracture toughness and associated fracture behaviour of bead-filled epoxy/glass fibre hybrid composites

JUNG JU LEE*
Department of Mechanical Engineering, KAIST, 373-1 Kusong-dong, Yusung-gu, Taejon 305-701, Korea
CHANG MIN SUH
Department of Mechanical Engineering, Kyung-pook National University, Taegu, Korea

To investigate enhancement of matrix-dominated properties (such as interlaminar fracture toughness) of a composite laminate, two different bead-filled epoxies were used as matrices for the bead-filled epoxy/glass fibre hybrid composites. The plane strain fracture toughness of two different bead-filled epoxies have been measured using compact tension specimens. Significant increases in toughness were observed. Based on these results the interlaminar fracture toughness and fracture behaviour of hybrid composites, fabricated using bead-filled epoxy matrices, have been investigated using double cantilever beam and end notch flexure specimens for Mode I and Mode II tests, respectively. The hybrid composites based on carbon bead-filled matrix shows an increase in both G_{Ic} initiation and G_{IIc} values as compared to a glass fibre reinforced plastic laminate with unmodified epoxy matrix. The optimum bead volume fraction for the hybrid composite is between 15% and 20%. However, the unmodified epoxy glass-fibre composite shows a higher G_{Ic} propagation value than that of hybrid composites, due to fibre bridging, which is less pronounced in the hybrids as the presence of the beads results in a matrix-rich interply region.

1. Introduction

During the past decade, a large growth in the use of composite materials in aerospace, marine and other structural applications has been reported. Currently, this design trend towards composites is moving into diverse engineering structure (even into satellite components and space structure) in order to reduce structural weight [1–3].

However, one of the limiting features of composite materials in service is their tendency for matrix cracking either within a ply (e.g. transverse ply cracking) or between plies (delamination or interlaminar cracking). Because a critical design criterion for fibre-reinforced composites is a sufficient fracture energy absorption capability, which is highly dependent on the matrix-dominated properties, much attention has been concentrated on improving the fracture toughness of epoxy resins [4–7].

According to previous research, there are two basic approaches to improve the mechanical performance of current epoxy resin matrices. One is to use an alternative type of polymer, for example high toughness thermoplastics such as poly-ether-etherketone (PEEK) [8, 9], and the other is to modify existing epoxies. This second approach is attractive because epoxy matrices possess many advantageous properties except for their lack of toughness. In addition, a drawback with the thermoplastic approach is the high fabrication cost and material processing constraints, such as the problems of wetting the fibres [10, 11]. To toughen epoxies by a particulate route, we can consider two methods. Firstly, there are rubber-toughened epoxies which are the incorporation of an elastomer phase, such as carboxyl terminated butadiene-acrylonitrile (CTBN), in the glassy matrix. This rubber-toughening increases the toughness of the resin by orders of magnitude. However, a large increase in resin toughness does not give a proportional increase in composite toughness, and the rubber-toughened resins may also result in a reduction in strength, modulus and hot/wet performance [12–14]. Secondly, there are systems based on rigid inorganic particles reinforcement such as alumina, silica, glass bead. The major toughening effect of these ceramic particles was reported as a crack-pinning process [15–17]. This second approach also has some problems. Uniform mixing and even dispersion of a filler material is difficult, due to the high density of ceramic filler. The edge and surface of the particles can

* Author to whom all correspondence should be addressed.

0022–2461

be a major source of stress concentration and cause internal failure of the materials [18, 19]. Recent developments include the modification of epoxy matrix using polymer particulates (such as thermoplastic, polyvinylidene fluoride, and nylon 6 particles) or ceramic whiskers as an alternative to the method of rubber toughening [19–21]. While this ceramic whisker-toughening approach has been shown to be successful in increasing the matrix cracking threshold, there are safety hazards in processing whiskers, and this also appears to degrade the strength of the composite [21].

In this paper, as part of a wide programme concerned with using a different type of secondary reinforcement, organic polymer particles such as carbon and phenolic beads were used as toughening agent in contrast to the previous inorganic ceramic-whisker filler materials [21]. The effect of varying the volume fraction of different types of carbon and phenolic beads on the plane strain fracture toughness of pure epoxy resin has been investigated. Based on these results, firstly glass fibre hybrid composites were fabricated using an epoxy matrix toughened with carbon and phenolic beads. Secondly, the interlaminar fracture toughness of hybrid composites was evaluated to investigate interlaminar fracture behaviour and then the associated optimum bead volume fraction for enhancement interlaminar fracture toughness was also discussed.

2. Experimental procedure

2.1. Materials and processing

The epoxy resin system is based on Epikote 828 epoxy cured with hardener (Epikure NMA). Carbon and phenolic beads were used as toughening agent. Manufacturer's technical data for the beads indicate that the carbon beads have a specific gravity of 1.85 and a mean particle size of 20 μm, while the corresponding values for the phenolic beads are 1.18 and 15–20 μm, respectively. Carbon beads used in this study are highly compatible to resin and resistant to corrosion and chemicals. Phenolic beads are a high-temperature organic filler with high thermal stability and reactivity with resin [22].

Epoxy resin was heated at a temperature of 40 °C for 15 min in order to facilitate mixing and stirring, and then the beads were dispersed in the resin at volume fractions of up to 40% by magnetically stirring. The resin/bead mixture was degassed, poured into an aluminium mould and cured at 100 °C for 3 h and then post-cured at 150 °C for 3 h.

To fabricate composite laminates with a bead-filled matrix, glass fibre was wound on to four metal frames. The resin/bead mixture was introduced at the top and bottom of the stack of frames and at each interface. The resin has to be applied at each interface because there is a tendency for the glass fibres to filter out the beads (Fig. 1). A thin (13 μm) layer of PTFE material was located at the midplane to provide a starter crack in the double cantilever beam (DCB) and end-notch flexure (ENF) specimens. The laminate was then cured at 100 °C for 3 h and post-cured at 150 °C for 3 h. The cured thickness of the laminate was 4 mm, although this depended slightly on the bead volume fraction, as did the volume fraction of glass fibre in the laminate. For instance, for epoxy resin with 15% by volume of bead, the volume fraction of glass in the laminate, V_f, was 52%, while for resin with 30% by volume of bead, V_f was 46%.

2.2. Compact tension tests

Nine compact tension specimens (CT) (Fig. 2) were made from each moulded plaque of bead-filled epoxy, so

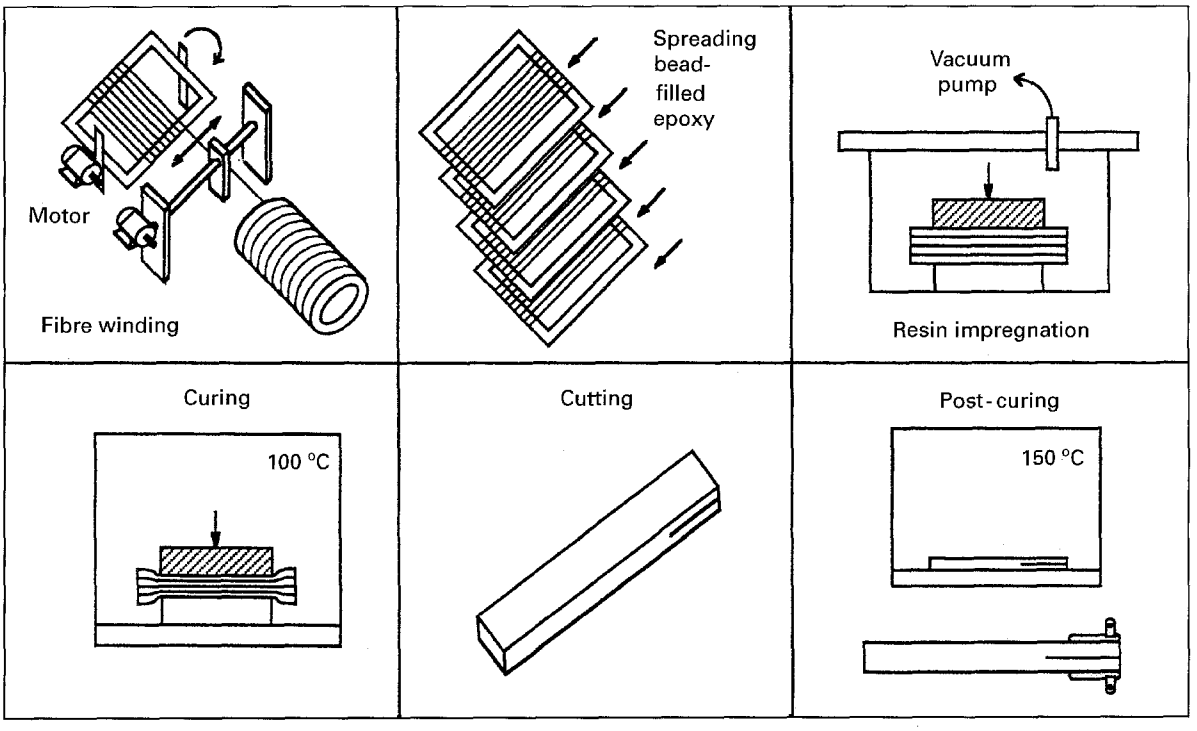

Figure 1 Schematic diagram of steps in the laminate fabrication process.

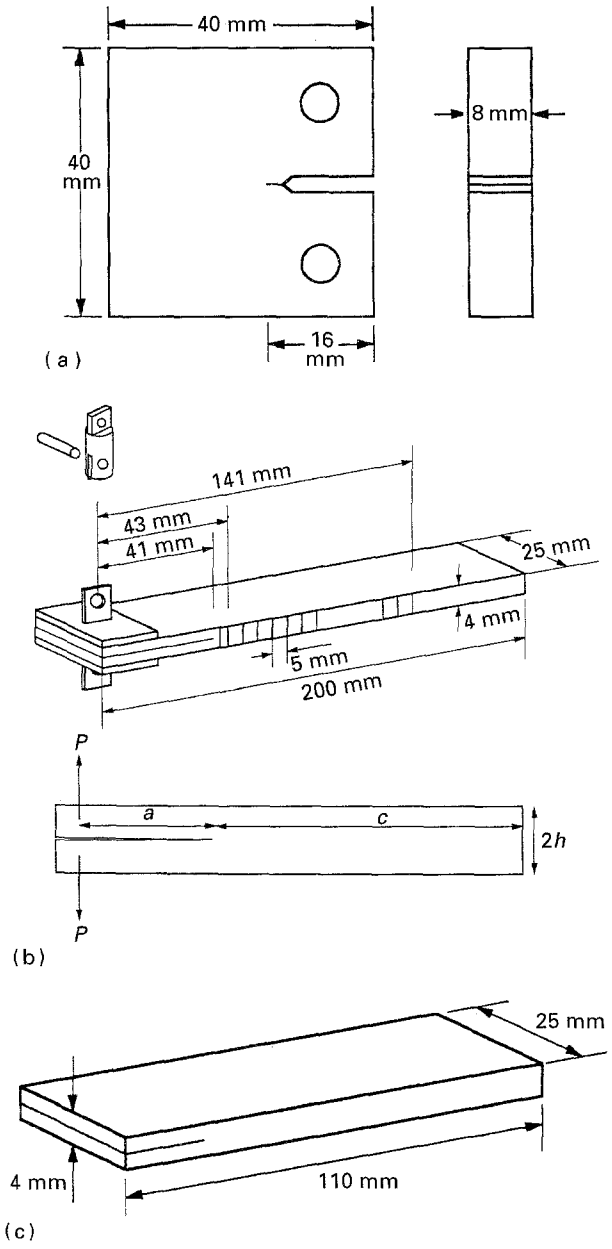

Figure 2 Dimensions of (a) CT, (b) DCB and (c) ENF specimens.

that fracture toughness, K_{IC}, values obtained in this study are a mean value from nine specimens. For precracking of compact tension specimens in polymeric materials, a razor blade is often used to sharpen a machined notch. However, this method can cause unacceptable scattering of K_{IC} data because of the variation in orientation and sharpness of precracks when many specimens are used. In this study, over one hundred compact tension specimens were used to obtain and compare K_{IC} data of many specimens with different bead volume fractions. To minimize these precrack problems, the precrack was moulded around a sharp insert during processing [23]. Plane strain fracture toughness values, K_{IC}, at the onset of crack propagation were obtained from the load–displacement curves using the following relationship (ASTM E399).

where P_f, B, W and a are the maximum load, specimen thickness, specimen width and crack length, respectively. The fracture energy (or critical energy release rate) was determined from the K_{IC} value using the following equation

$$G_{IC} = K_{IC}^2/E \tag{2}$$

where the value of E was determined using bend tests [24].

2.3. DCB tests

2.3.1. Specimen details

DCB specimens (Fig. 2), 200 mm long, 25 mm wide and 4 mm thick, were machined from the unidirectional hybrid composite panel. Aluminium alloy end blocks were bonded to the end of the specimens containing the PTFE inserts and load was applied via pins through holes in the blocks.

2.3.2. Data reduction methods for DCB tests

The G_{IC} values obtained in this study were calculated by an experimental compliance method [25] using Equation.

$$G_{IC} = \frac{nP\delta}{2Ba} \tag{3}$$

where P is the applied load, δ is the displacement, B is the specimen width and a is the crack length. The coefficient, n, is found from the slope of a log–log plot of compliance against crack length. As an alternative fracture toughness value to the G_{IC} analysis described above, it is possible to obtain K_{IC} values. Foote and Buchwald [26] have reported an exact solution for the stress intensity factor for the DCB specimen based on isotropic stress analysis

$$K_{IC} = \frac{P}{Bh^{1/2}}\{(12)^{1/2}(a/h + 0.673) + [(2h/\pi a)]^{1/2} - [0.815(a/h)^{0.619} + 0.429]^{-1}\} \tag{4}$$

Equation 4 is valid for all values of a/h, provided that $c/h > 2$ where c and h are the uncracked ligament size and thickness of one arm of the beam, respectively (i.e. total beam thickness is $2h$). In this study, $a/h < 40$ with $c/h > 2$, and Equation 4 is thus valid for the DCB specimens used in this study and has been used by other researchers testing composite laminate DCB specimens [27]. There is also a well-known analysis based on a simple beam theory which is

$$K_{IC} = (12)^{1/2} Pa/Bh^{3/2} \tag{5}$$

Equation 5 has been used by Newas [28] to analyse carbon/PEEK laminates.

$$K_{IC} = (P_f/BW^{1/2})\,F(a/W) \tag{1a}$$

$$F(a/W) = \frac{(2 + a/W)(0.886 + 4.64\,a/W - 13.32\,a^2/W^2 + 14.72\,a^3/W^3 - 5.6\,a^4/W^4)}{(1 - a/W)^{3/2}} \tag{1b}$$

2.4. ENF tests

ENF specimens (Fig. 2), 110 mm long by 25 mm wide, were machined from the same panels as the DCB specimens. The load and displacement at the onset of crack propagation enables the interlaminar toughness, G_{IIC}, to be determined from beam theory [25, 29].

$$G_{IIC} = \frac{9P\delta a^2}{2B(2L^3 + 3a^3)} \quad (6)$$

where L is the half-span of specimens loaded in three-point bending.

2.5. Experimental details

All mechanical tests were carried out at ambient temperature using a displacement-controlled Instron 1175 testing machine. Compact tension tests were performed at a constant displacement rate of 0.5 mm min^{-1} using a compact tension test jig. DCB and ENF tests were performed at a constant displacement rate of 2 mm min^{-1}. To monitor the position of the crack front, one edge of the specimen was coated with a white brittle fluid and fine marks were put on this edge at 5 mm intervals to aid measuring the crack length. The load–displacement graphs were recorded on an X–Y plotter. Fracture surfaces of the specimens were coated with a thin layer of gold to make their surfaces conductive and so reduce charging when examined subsequently in a scanning electron microscope (SEM).

3. Results

3.1. Effect of phenolic and carbon beads on the K_{IC} values as a function of bead volume fraction

Fig. 3 shows the relationship between the fracture toughness value, K_{IC}, and volume fraction of carbon beads and phenolic beads, and the corresponding G_{IC} data are shown in Fig. 4. The error bars in Fig. 3 show one standard deviation on either side of the mean value. From Figs 3 and 4 it can be said that the volume fraction of carbon and phenolic beads has a significant effect on the K_{IC} value. Such a trend has been well documented in the related literature for a range of epoxy resin and filler materials [16, 18]. From Fig. 3, we find that the relationship between

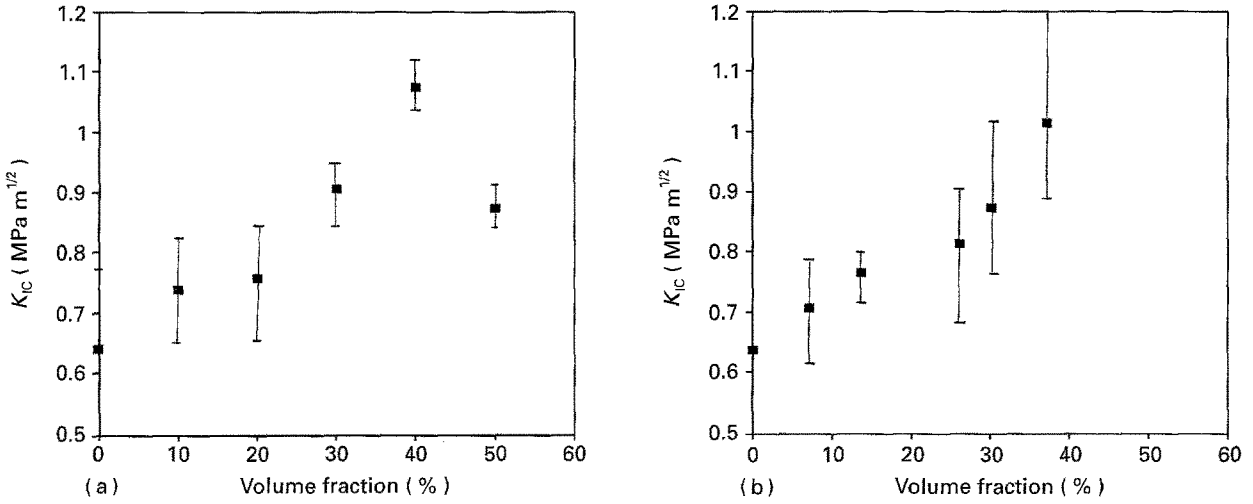

Figure 3 Fracture toughness of compact tension specimens of epoxy resin as a function of volume fraction of bead reinforcement (a) carbon beads, (b) phenolic beads.

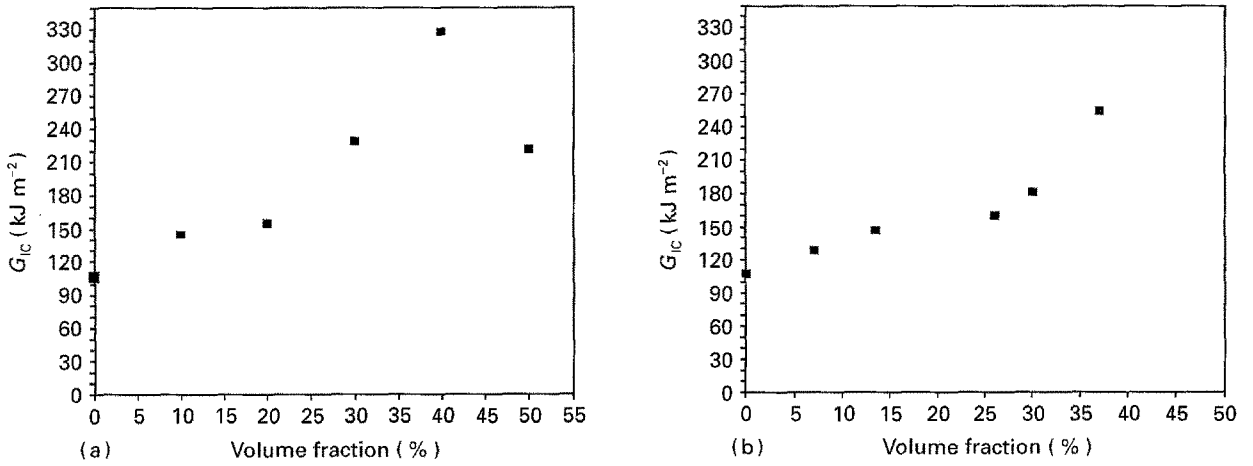

Figure 4 Critical strain energy release rate of compact tension specimens of epoxy resin as a function of volume fraction of bead reinforcement: (a) carbon beads, (b) phenolic beads.

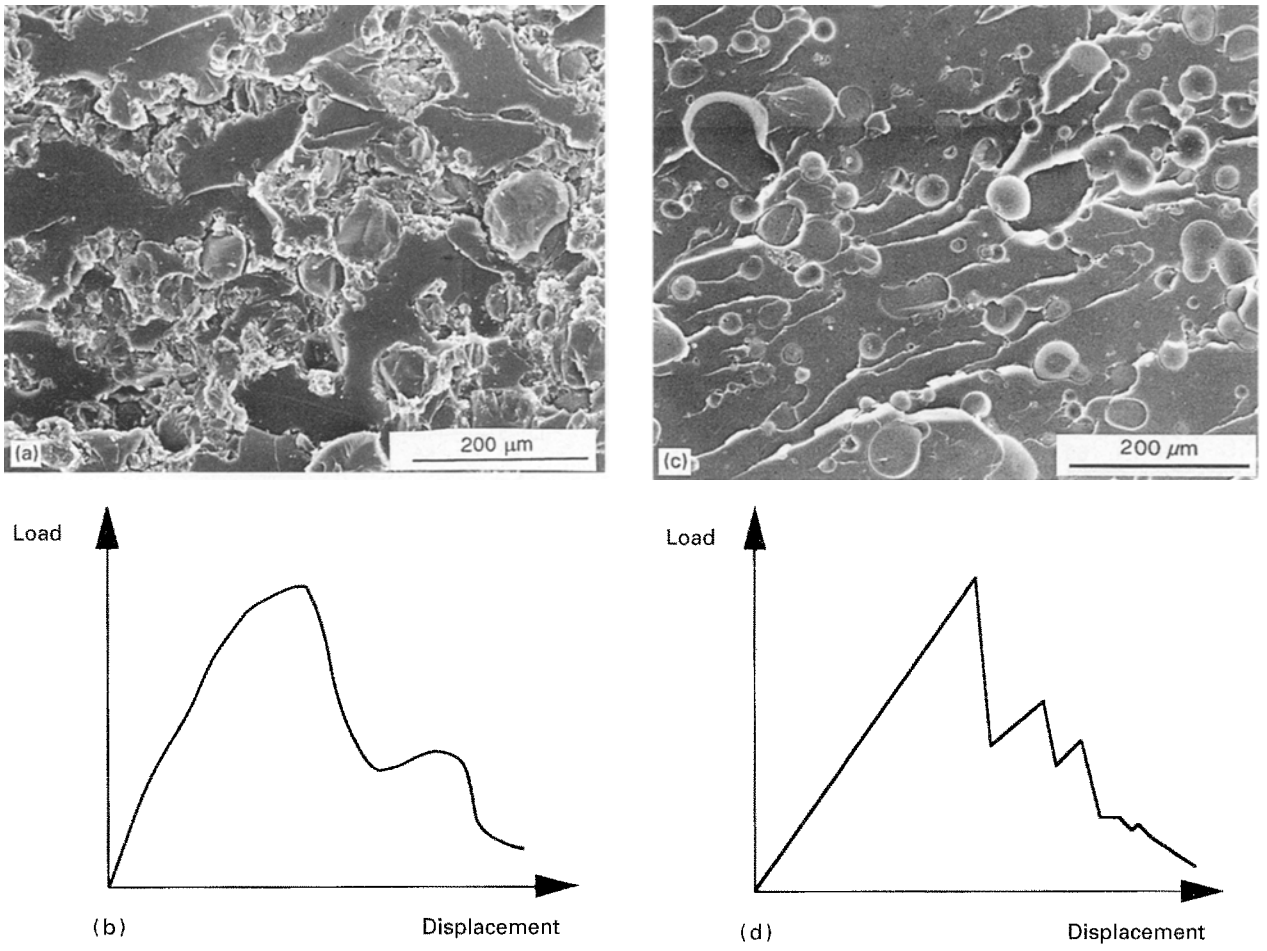

Figure 5 Scanning electron micrographs of a compact tension (CT) specimen fracture surface and corresponding schematic load–displacement records (a) fracture surface of carbon bead-reinforced epoxy (30% bead volume fraction) showing evidence of local deformation around the particles and transparticle fracture, (b) load–displacement record of carbon bead-reinforced epoxy CT specimen, (c) fracture surface of phenolic bead-reinforced epoxy (30% bead volume fraction) showing evidence of crack pinning, (d) load–displacement record of phenolic bead-reinforced epoxy CT specimen.

K_{IC} value and volume fraction of phenolic beads is reasonably linear within the scatter. The fracture toughness of carbon bead-filled epoxies increased with the increase of bead volume fraction up to 40% and then decreased sharply as shown in Fig. 3. It seems that the reduction of the K_{IC} value after 40% was caused by material processing problems, implying that there may be material mixing problems leading to the occurrence of voids at high volume fractions. Representative scanning electron micrographs of the fracture surface of carbon and phenolic bead-filled epoxy systems are shown in Fig. 5.

3.2. Mode I interlaminar fracture toughness of hybrid composites

3.2.1. Compliance/crack length relation

Fig. 6a shows the compliance variation with crack length for specimens with different volume fractions of carbon beads in the epoxy resin matrices. The same data were plotted on log–log scales in Fig. 6b. The data shown in Fig. 6a and b are the average from five specimens and typical examples (for the mean value of five specimens) is shown in Fig. 6c, d. In Fig. 6a, a comparison of the compliance-crack length data for different volume fractions of hybrid composites is shown. The plots show that at any given crack length, the compliance increases with increasing bead volume fraction. This is a consequence of the reduced fibre volume fraction (to maintain the same thickness of specimens, i.e. 4 mm) at the large bead volume fractions and an associated reduction in flexural stiffness.

It can be seen from the log–log plots (Fig. 6b) that the slope is very close to 3, which is necessary to justify using the compliance method to determine G_{IC}. The slope for the 15% hybrid composite material is almost exactly 3. A very slight deviation from 3 can be observed for the pure epoxy glass-fibre composite and for the 30% hybrid composite material. However, it can be said that the slopes observed are all acceptably close to the theoretical value, i.e. 3.

3.2.2. Interlaminar fracture toughness results

The results from the DCB test carried out on four bead-reinforced epoxy resin-based GFRP laminates (at bead fractions of 10%, 15%, 20%, and 30% by volume of matrix) and the baseline pure epoxy matrix laminates are shown in Fig. 7a as plots of G_{IC} from

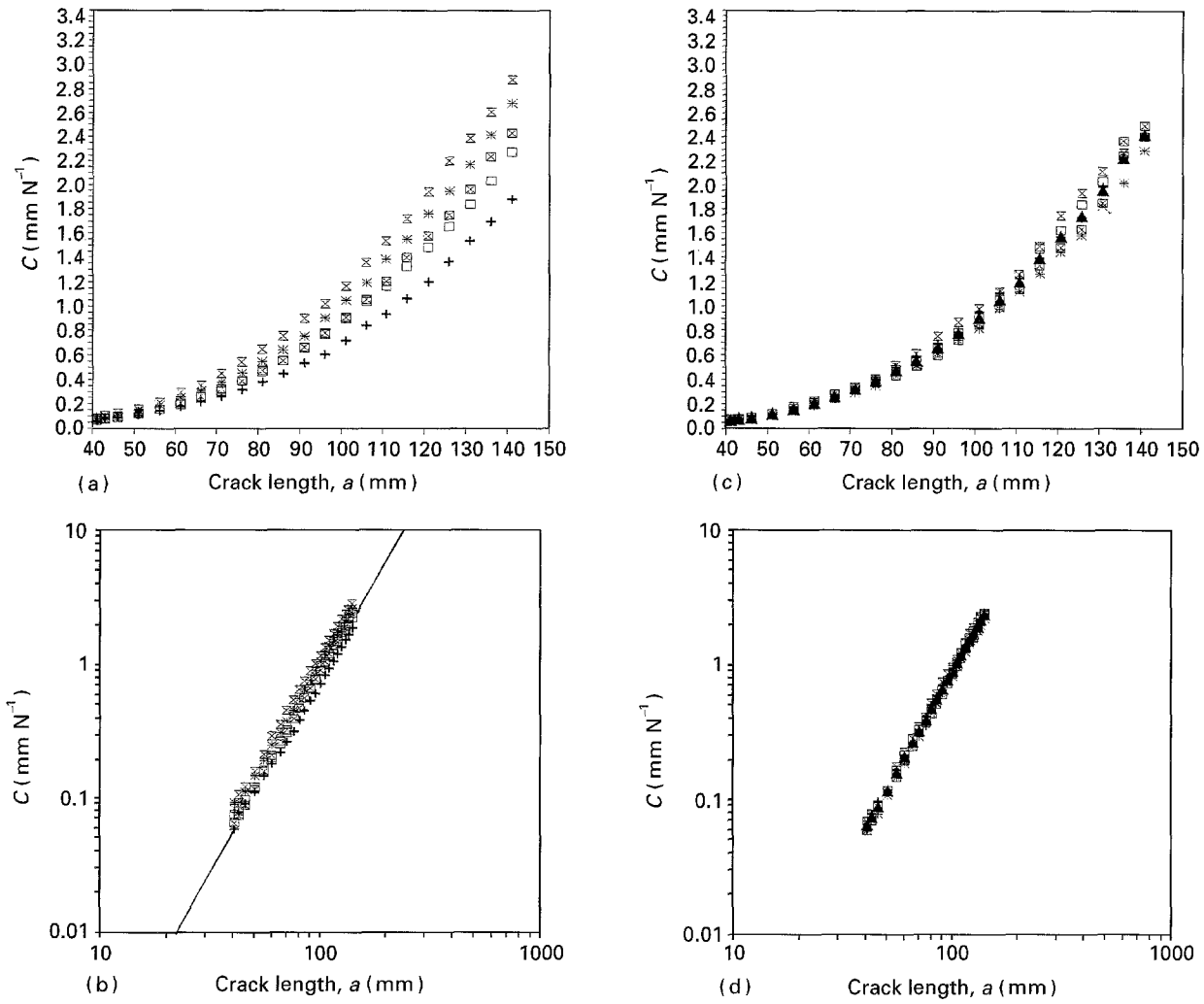

Figure 6 Plots of compliance against crack length, a, for DCB specimens of hybrid composite laminates with carbon bead volume fraction in the range 0%–30% by volume of matrix: (a) linear scale, (b) log–log scale with solid line representing an ideal slope of 3, (c) plots of compliance, C, versus crack length, a, for 15% hybrid composite showing a mean value of five specimens (linear scale), (d) plot of compliance, C, versus crack length, a, for 15% hybrid composite showing a mean value of five specimens (log–log scale). (+) Unmodified epoxy, (□) 10%, (⊠) 15%, (*) 20% and (*) 30% carbon bead-filled hybrid, (x) mean value.

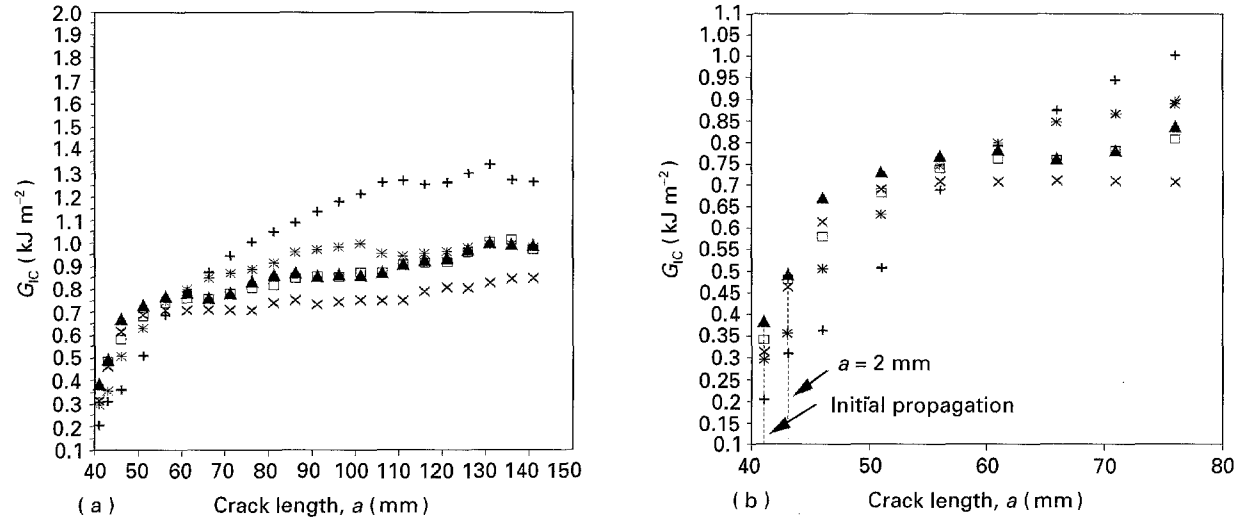

Figure 7 Plots of G_{IC} values as function of crack length, a, for DCB specimens of hybrid composite laminates with carbon bead volume fraction in the range 0%–30% by volume of matrix: (a) showing the whole crack propagation behaviour, (b) showing early stages of crack propagation in detail. (+) Unmodified epoxy, (*) 10%, (□) 15%, (▲) 20% and (×) 30% carbon bead-filled hybrid.

Equation 3 versus crack length. For each material, five specimens were tested. In every case, the G_{IC} values associated with the onset of crack growth, $G_{IC\ init}$, are different from those of the subsequent G_{IC} growth values, i.e. the materials show a rising R-curve.

The value of $G_{IC\ init}$ at the onset of crack growth was evaluated in two ways, as shown in Fig. 7b. The first

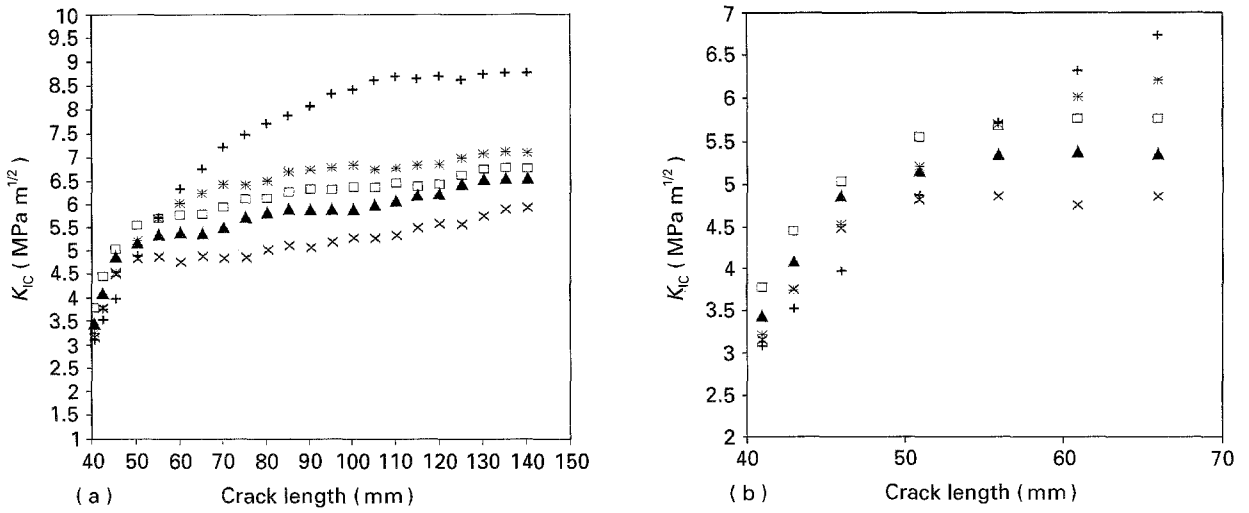

Figure 8 Plots of K_{IC} values as function of crack length, a, for DCB specimens of hybrid composite laminates with carbon bead volume fraction in the range 0%–30% by volume of matrix: (a) showing the whole crack propagation behaviour, (b) showing early stages of crack propagation in detail. (+) Unmodified epoxy, (∗) 10%, (□) 15%, (▲) 20% and (×) 30% carbon bead-filled hybrid.

value was calculated based simply on the load at which initial crack propagation from the insert occurs. After a 2 mm increment of crack growth the specimens were unloaded and then loaded again to obtain a second $G_{IC\ init}$ value corresponding to a 2 mm increment of crack growth ahead of the insert [30]. This latter method is a means of avoiding problems arising from the fibre disturbance and the resin-rich region usually associated with the presence of the insert. Both methods of determining $G_{IC\ init}$ gave higher values for the hybrid composites than for the pure epoxy glass-fibre composite, as shown in Fig. 7b. However, after crack extension to a crack length of greater than about 60 mm the subsequent, G_{IC} propagation value of the GFRP laminates based on unmodified epoxy is higher than that of any of the hybrid composites. Fig. 7b enables values for the initiation and early stage of crack propagation to be compared more clearly.

The effect of bead volume fraction on the $G_{IC\ init}$ value is not consistent with that on the subsequent G_{IC} propagation value. The G_{IC} initiation value at 20% beads by volume shows the highest value of the five different composites. However, the subsequent G_{IC} propagation values of the 20% hybrid composite are lower than those of both the pure epoxy and the 10%, 15% hybrid composites. These results were associated with the fracture mechanisms in these materials and will be explained with the aid of fractographic analysis, see Fig. 11.

The crack growth resistance calculated from Equation 4 in terms of the critical stress intensity factor, K_{IC}, of the composites with pure epoxy and different volume fractions of bead-reinforced matrices, are shown in Fig. 8a and b as plots of K_{IC} versus crack length, a. Again, each plot shows the results for five specimens and the mean value. The general trend of the K_{IC} curves is similar to the G_{IC} curves except that the hybrid composite fabricated with a reinforced matrix with 15% by volume of beads shows the highest K_{IC} initiation value, Fig. 8b. Interestingly, the peak initiation values of G_{IC} and K_{IC} do not occur at the same bead volume fractions; also the peak value of

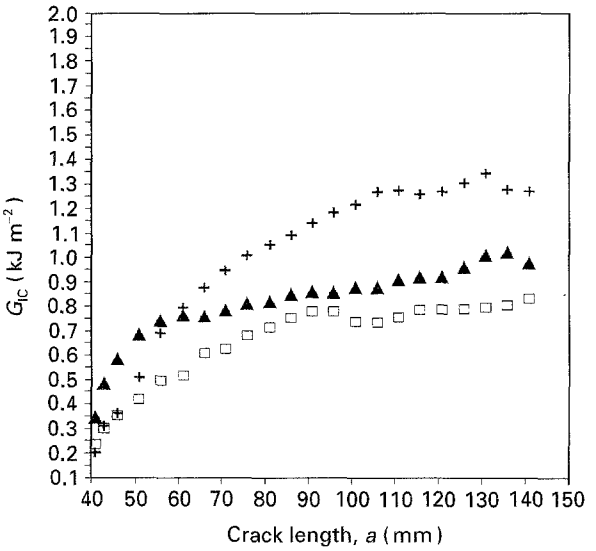

Figure 9 Comparison of interlaminar fracture toughness, G_{IC}, as a function of crack length, a, for DCB specimens of (+) unmodified epoxy/glass fibre composite and hybrid composite laminates based on 15% (▲) carbon and (□) phenolic beads.

toughness in each case occurs at a lower bead volume fraction than for the neat resin (Fig. 3). Finally, Fig. 9 enables the R-curve behaviour of the unmodified epoxy composite and carbon-bead hybrid composites to be compared with data obtained from hybrid composites with phenolic beads at the same bead volume fraction (15%). The behaviour of the phenolic bead system is poor compared to the carbon beads. There is no significant enhancement in the G_{IC} initiation value of phenolic bead hybrid composites compared to the pure epoxy system and the R-curve behaviour is less pronounced.

3.3. Mode II interlaminar fracture toughness of hybrid composites

The Mode II interlaminar fracture toughness values (determined from the ENF tests) are shown as a function of bead volume fraction in Table I and Fig. 10.

TABLE I Toughness properties for carbon bead-filled epoxies and associated hybrid composites

Material	Matrix	Composite properties		
	G_{IC} (J m^{-2})	G_{IC} (init.) (J m^{-2})	G_{IIC} (J m^{-2})	G_{IIC}/G_{IC}
Unmodified epoxy	105	208	1600	7.7
Epoxy with 10% beads	135	295	1930	6.5
Epoxy with 15% beads	143	340	1970	5.8
Epoxy with 20% beads	150	380	1210	3.2
Epoxy with 30% beads	225	315	–	–

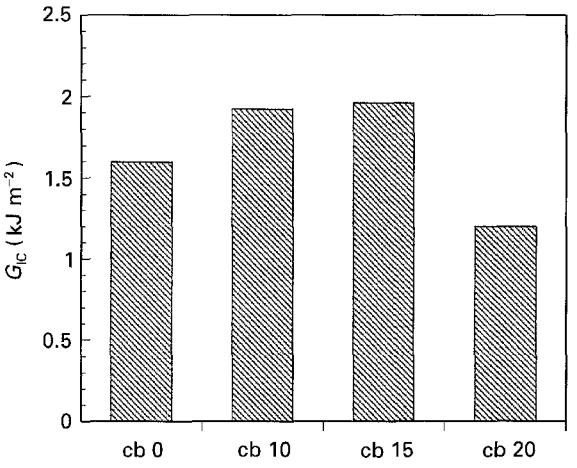

Figure 10 Comparison of G_{IIC} values of hybrid composite in the range 0%–30% by volume of matrix. cb O, pure epoxy matrix; cb 10, 10% carbon bead-filled epoxy matrix composite; cb 15, 15% carbon bead-filled epoxy matrix composite; cb 20, 20% carbon bead-filled epoxy matrix composite.

The data indicate that there is a peak toughness at a volume fraction of 15% but that there is a decrease thereafter, so that at high volume fractions the toughness is less than the laminate based on the unmodified epoxy. Representative Mode II fracture surfaces from the unmodified epoxy system and a hybrid composite are shown in Fig. 12 below.

3.4. Fractographic analysis and fracture mechanism

3.4.1. Fractographic analysis

In Fig. 5, scanning electron micrographs of the fracture surface of the carbon and phenolic bead-filled epoxies without fibres is shown. The fracture surfaces of carbon bead-filled epoxy show very irregular crack paths due to multi-level cracking, transparticle fracture and localized plastic deformation, Fig. 5a. Typical crack-pinning evidence [16, 17] showing characteristic tails and steps, is observed in Fig. 5b. Scanning electron micrographs of the fracture surface of the unmodified epoxy and bead-filled matrix hybrid composites from the Mode I DCB test specimens, are shown in Fig. 11. A large amount of fibre bridging can

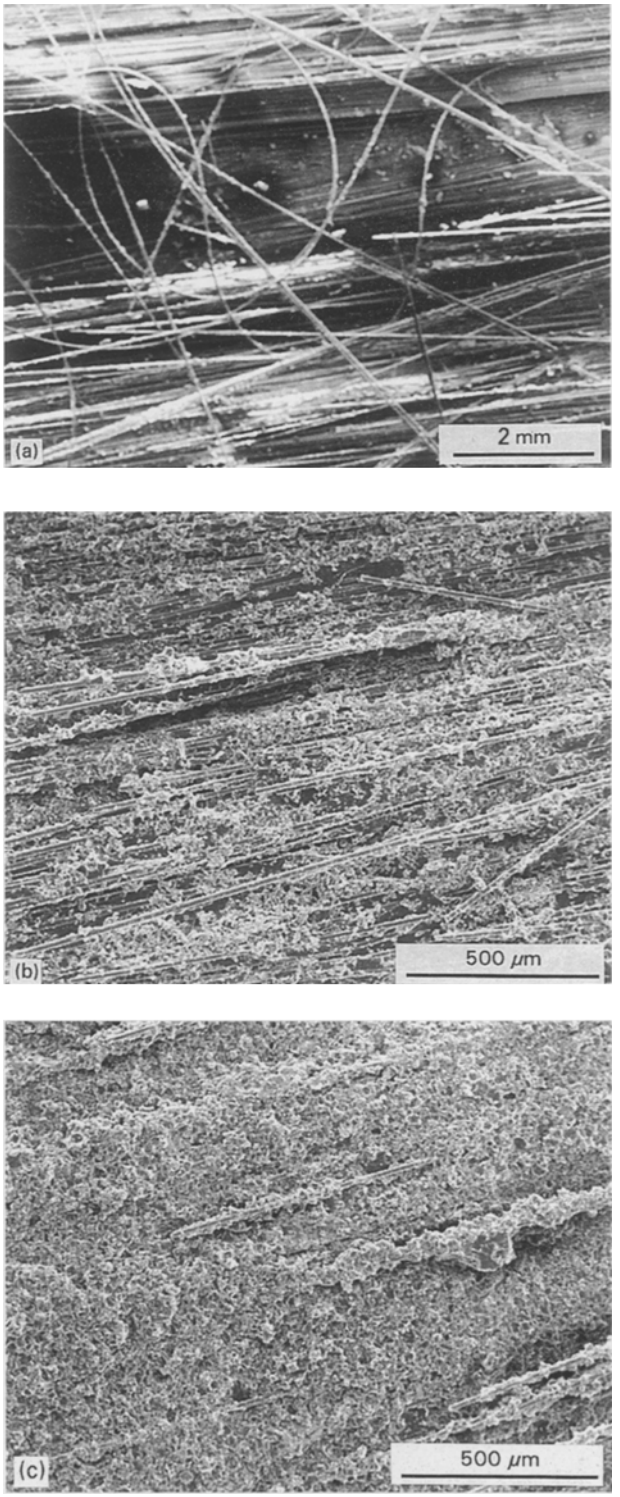

Figure 11 Scanning electron micrographs of DCB fracture surface of hybrid composite laminates showing greater coverage of fibres by matrix, and hence less fibre bridging during crack growth, with increasing bead fraction: (a) unmodified epoxy/glass fibre composite, (b) hybrid composite 15% carbon bead by volume of matrix, (c) hybrid composite, 30% carbon bead by volume of matrix.

be seen on the fracture surface of the pure epoxy glass-fibre composite as shown in Fig. 11a. Increasing bead volume fraction decreases the degree of fibre bridging as shown in Fig. 11b and c. From the many other scanning electron micrographs, it can be summarized that the fracture surface of carbon bead-reinforced hybrid composite is characterized by fibre bridging as well as fibre debonding, pull-out and

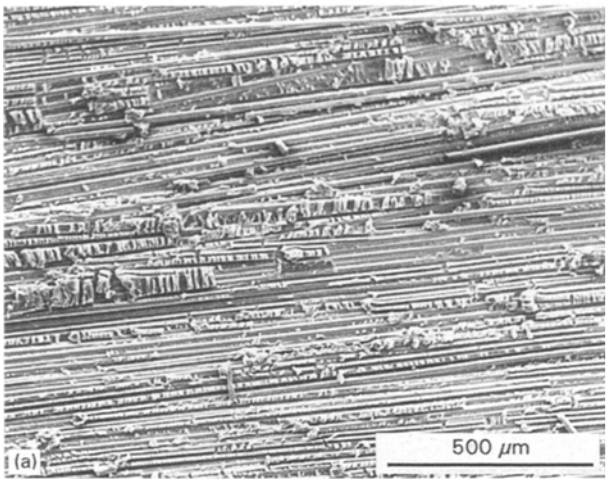

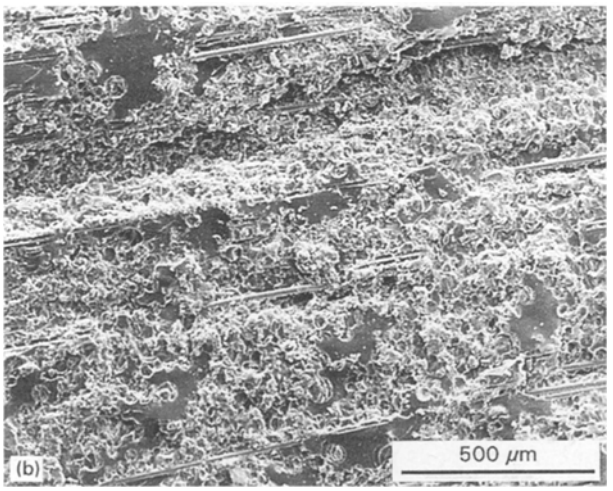

Figure 12 Scanning electron micrographs of ENF fracture surface of hybrid composite laminates: (a) unmodified epoxy/glass fibre composite, (b) hybrid composite, 15% carbon bead by volume of matrix, (c) hybrid composite, 20% carbon bead by volume of matrix.

transparticle fracture of the carbon beads and associated plastic deformation. The fracture surface of phenolic bead-reinforced hybrid composite shows a similar fibre-related fracture surface but the tails characteristic of crack pinning (which were observed clearly in phenolic bead-reinforced epoxy without fibre) are not now observed.

Scanning electron micrographs of the fracture surfaces of ENF specimens are shown in Fig. 12. Compared with the DCB specimens there is little fibre bridging in the ENF specimens. This can be seen by comparing Fig. 12 with Fig. 11. In fractographs of pure epoxy glass-fibre composite (Fig. 12a), many uneven looking facets (called hackles [31]) can be seen. The distinctive nature of these features decreases with increasing bead volume fraction in the matrix, as shown in Fig. 12.

3.4.2. Fracture mechanism

The detailed observations made on the carbon bead-filled composites may be summarized as follows.

(a) Interlaminar crack propagation occurs largely at the fibre–matrix interface, rather than in the resin in the pure epoxy/glass fibre composite. With increasing bead volume fraction, there is a trend away from this, with the crack path increasingly following resin-rich regions.

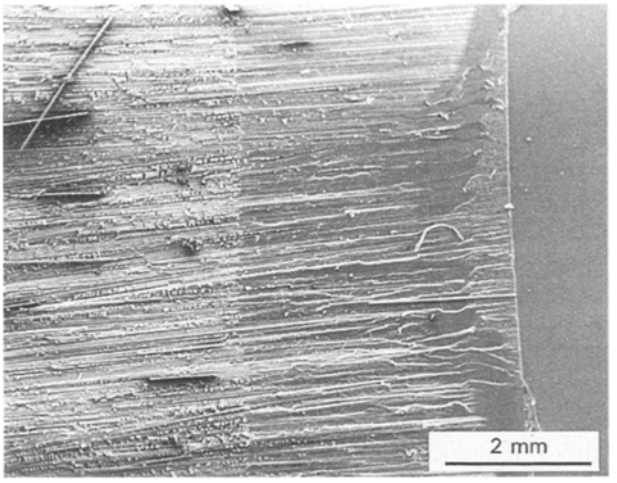

Figure 13 Fracture surface of ENF specimen of pure epoxy glass fibre composite in the SEM, showing differences between Mode I (right side) and Mode II (left side) crack path.

(b) Interlaminar crack growth leads to fibre bridging, debonding, breakage and pull-out behind the crack tip. A large number of fibres link across the Mode I crack from one half of the beam to the other, so forming a bridge, as shown in Fig. 11. The degree of fibre bridging depends on the bead volume fraction (with higher volume fractions leading to less bridging).

(c) The presence of carbon beads in neat resin samples was shown to localize plastic deformation (leading to crack-tip blunting, Fig. 5) prior to fracture of the particle. A similar mechanism seems to operate when the bead is incorporated into the matrix of the composite DCB specimen because fractured beads are seen on the fracture surface.

In Fig. 13, the fracture surface of both Mode I and Mode II crack growth is seen simultaneously. The contrast between Mode I and Mode II fracture surfaces is due to different fracture mechanisms. Bradley [31, 32] has described in detail the fracture mechanisms of Mode I and Mode II interlaminar crack growth using *in situ* observations in the SEM. Mode I failure occurs with the development of a small deformation zone ahead of the crack tip, as *evidenced* by the considerable microcracking in the scanning electron micrograph. On the other hand, Mode II delamination crack growth begins with the formation of a series of sigmoidal-shaped matrix microcracks ahead of the crack tip with an orientation of approximately 45° to the fibre direction (which for Mode II loading is the principal tensile stress plane). Similar features have been observed in this work. The fracture surfaces of Mode I DCB specimens suggest that the crack growth in Mode I occurs principally along the resin/fibre interface. By contrast, it leaves the Mode II delamination fracture surface with many "hackles", as shown in the fractographs of the hybrid composites, Fig. 12.

4. Discussion

4.1. Fracture mechanics parameters for bead-filled epoxies

The fracture toughness values, K_{IC} and G_{IC}, of bead-filled epoxies as a function of bead volume fraction for

the carbon and phenolic bead-filled systems, are shown in Figs 3 and 4. Because the effect of the bead on the composite modulus is small, the trend in G_{IC} is broadly similar to that of K_{IC}. The dependence of G_{IC} on K_{IC}^2 means that for both systems the percentage change of G_{IC} with bead volume fraction is larger than the corresponding change in K_{IC}. This effect is slightly larger in the carbon system where the decrease in modulus with bead volume fraction, although a small effect, adds to the large increase in G_{IC} caused by the increase in K_{IC}. In systems based on inorganic fillers, a quite different behaviour is seen [17, 18]. In such systems, the trends of variation of the energy release rate, G_{IC}, are quite different from that of fracture toughness, K_{IC}. These differences are caused by the large increase of modulus of the particle-filled epoxies with increase of particle volume fraction. This can lead to the modulus rising at a faster rate than K_{IC}^2 with increasing volume fraction of filler, so that the value of G_{IC} will go through a maximum and then fall.

Examination of the fracture surfaces in the SEM showed quite different behaviour in the two systems. In the carbon bead-filled system (Fig. 5), the fracture surface is rough with only a few of the "tails and steps" features usually taken as indicative of toughening by a crack-pinning mechanism. It has been reported [16] that the absence of tails does not necessarily mean that crack pinning does not occur, because at high volume fraction of particles there may be considerable overlaps of secondary cracks. We suggest, however, that for the carbon bead-filled material, the greater degree of roughness is associated with plastic deformation. This is consistent with the load–displacement records, Fig. 5b, obtained, in that the round peaks seen may correspond to progressive failure of the interface and localized plastic deformation of the matrix around the particles [24]. An additional feature of the fracture surface was the presence of fractured particles, Fig. 5a. There appears to be a strong interfacial bond between the particle and matrix and the energy required to stretch and fracture the particle can make a significant contribution to the toughness. In the phenolic bead-filled system, however (Fig. 5c), the "tails and steps", generally taken as characteristic of crack pinning, can be seen. Hence, crack pinning (or more precisely multi-level cracking as the secondary cracks propagate between the particles and subsequently link up), is identified as the major toughening mechanism in this system. The corresponding load–displacement behaviour was "brittle–unstable" [23, 33] with a sharp load peak, Fig. 5(d).

4.2. Mode I interlaminar fracture toughness tests

4.2.1. G_{IC} values from DCB tests

A comparison of Figs 7 and 8 shows that the highest K_{IC} and G_{IC} initiation values occur at different volume fractions of bead. The highest G_{IC} values occurs at a volume fraction of 20%, whilst the highest K_{IC} value occurs at 15%. This can be explained by considering Equations 3 and 4, from which G_{IC} and K_{IC}, respectively were calculated. In Equation 3, the important variables are load, P, and displacement, δ, but in Equation 4, only the load, P, appears. The 15% hybrid composite showed the highest crack initiation load, P. The K_{IC} value, which is independent of the displacement of the laminate, is thus the highest value of all five materials from the 15% hybrid composite. But the 20% hybrid composite showed a higher displacement compared to 15% hybrid composite, although the crack initiation load is slightly lower than that of the 15% hybrid composite in the load–displacement record obtained in this study. Consequently, the 20% hybrid composite shows the higher G_{IC} value, which depends on the product of load, P, and displacement, δ. The materials containing nominally 15% and 20% by volume of carbon bead in the matrix showed higher toughness than the 30% material, even though the 30% material was tougher when tested as a bead-filled epoxy without the fibres (Fig. 3). One possible explanation for this is that the nominal bead volume fractions will certainly be underestimates of the actual bead volume fraction present in the plane of propagation of the interlaminar crack, due to the fibres preventing the beads from being distributed uniformly within the matrix. Hence the interlaminar toughness will not correspond to those of bead-filled epoxies where the distribution of beads is much more uniform.

In the early stages of crack growth, the hybrid composites show higher G_{IC} (and K_{IC}) values than the unmodified epoxy glass-fibre composite (Figs 7 and 8). However, after crack extension to a crack length of greater than about 60 mm, the subsequent G_{IC} (and K_{IC}) propagation values of the GFRP laminates based on unmodified epoxy are higher than those of any of the hybrid composites. This is a result of fibre bridging occurring in this material to a greater extent than in the hybrid laminates, as shown by the different appearance of the fracture surfaces. A large amount of fibre bridging can be seen on the fracture surface of the unmodified epoxy glass fibre composite, Fig. 11a. In the hybrid composite laminates the presence of the beads leads to a bead-rich interlayer and the interlaminar crack remains largely within this layer, especially in the 30% laminate, as shown in Fig. 11c. Consequently, there is less bridging in the 15% material, Fig. 11b, and there was very little in the 30% material, Fig. 11c. It was also seen that the transparticle fracture mechanism operates in the hybrid composites, as in the compact tension specimens.

In Fig. 9, the R-curve behaviour of a hybrid composite fabricated with carbon bead-reinforced matrix is compared with that of a hybrid composite reinforced by phenolic beads at the same bead volume fraction (15%). The G_{IC} initiation and propagation values of carbon bead-reinforced hybrid composite are both higher than those for the phenolic bead-reinforced hybrid composite. The fracture surface of the carbon bead-reinforced hybrid composite showed fibre bridging as well as fibre debonding and pull-out and transparticle fracture of the carbon beads and associated plastic deformation leading to crack-tip

blunting. The fracture surface of the phenolic bead-reinforced hybrid composite showed similar fibre bridging to the carbon bead hybrid composite (as might be expected) but the features characteristic of "crack pinning" (which were observed clearly in phenolic bead-reinforced epoxy without the fibre), are not now observed. The conclusion of this comparison is that the toughening mechanisms associated with the carbon bead in the matrix alone are relevant in the composite, while those associated with the phenolic bead are not, possibly because "pinning"-type effects associated with the fibres are more important than those arising from the bead.

4.2.2. Optimum bead volume fraction for mode I toughness

G_{IC} and K_{IC} values of five different composite laminates (pure epoxy glass fibre and four different hybrid composites fabricated with 10%, 15%, 20%, 30% bead-reinforced matrix) have been compared and each composite system shows a slightly different G_{IC} and K_{IC} behaviour as shown in Figs 7 and 8. Before we comment on the optimum bead volume fraction, we have to comment on the relevance of the initiation and the propagation values. DCB specimens used in this study were not fabricated from commercial prepreg but using a filament winding technique (Fig. 1) which is useful for laboratory-level fabrication of specimens of different matrix systems. The interface between plies of a laminate fabricated using the filament winding method, is considerably rougher due to the nature of the winding process.

Fibre bridging is generally attributed to the nesting of fibre and weak fibre–matrix interfaces. When two plies of the same orientation are adjacent to each other in the laminate, the cure pressure forces the plies to merge together and removes the characteristic thin layer of resin between plies. In our fabrication method, merging of fibres can take place more easily compared to the prepreg method leading to more fibre bridging. However, if we introduce beads into the matrix, the extent of the thin layer of bead-rich resin between the plies of the laminate increases with increasing bead volume fraction, because the fibre prevents the beads from evenly distributing within the plies. The beads tend to inhibit fibre bridging and, consequently, the amount of fibre bridging decreases with increasing bead volume fraction in the matrix material, as shown in Fig. 11a–c. Therefore, the G_{IC} propagation value of the hybrid composites decreases with increasing bead volume fraction and pure epoxy glass-fibre composite shows the highest value of the five different composites. Close to the insert in the DCB specimen (around the area from which the G_{IC} initiation value is obtained), plies can be prevented from fibre nesting as a result of the presence of the insert. Hence, the condition of the interface between the plies becomes similar to that if the laminate had been fabricated from prepreg.

To summarize, it might be said that the G_{IC} initiation value obtained from the filament winding method using an insert would therefore be close to that of laminate manufactured using the prepreg method. On the other hand, the G_{IC} propagation value for pure epoxy glass fibre was considerably higher because of the additional fibre bridging. From an engineering design viewpoint, it might be said that the G_{IC} initiation value is more important than the G_{IC} propagation value of an established crack. In the light of the argument, the optimum bead volume fraction for maximizing the G_{IC} and K_{IC} initiation values is discussed below. The presence of the bead results in an increase in the initiation value of interlaminar toughness and fracture toughness G_{IC} and K_{IC}, compared to the standard epoxy laminate. The materials containing nominally 15% and 20% by volume of bead in the matrix showed higher toughness than the 30% material, even though the 30% material was tougher when tested as a bead-filled epoxy without the fibres. As indicated earlier, the nominal bead volume fractions in the composites will certainly be underestimates of the actual bead volume fraction present in the plane of propagation of the interlaminar crack so that the interlaminar toughness will not correspond to that of bead-filled epoxies where the distribution of beads is much more uniform. The observation of a peak toughness in the composite at a bead fraction of 15%–20% may indicate that at higher bead volume fractions a reduction in constraint associated with the increasing thickness of the bead-rich interlayer between the plies leads to a lower crack propagation load and hence reduced toughness.

4.2.3. Translation of resin toughness into composite Mode I interlaminar toughness

Table I enables the Mode I toughness for the glass fibre/carbon bead-filled epoxy composites to be compared with the toughness of the corresponding bead-filled matrix (note that this is not strictly a valid comparison because the volume fraction of beads at the interface in the composites will be higher than at the crack plane in the bead-filled epoxy compact tension specimens). The data indicate the effectiveness of the carbon-bead system in the range 10%–20% and the relatively poor result from the 30% carbon beads. The trends for the increase in G_{IC} values for the composites based on carbon beads at fractions of less than 30% are broadly in agreement with the data relating DCB composite toughness to matrix toughness, shown by Hunston and Dehl [34].

The reason why the interlaminar toughness value of the composite is higher than the value of G_{IC} of the neat matrix for values of matrix $G_{IC} < 400\ J\ m^{-2}$ has been explained by a number of factors [13, 32]. The most relevant is the additional surface area associated with the corrugated nature of the delamination fracture surface and fibre bridging behind the crack tip. There is often a lower efficiency of translation of resin fracture toughness into delamination fracture toughness for neat resin with $G_{IC} > 400\ J\ m^{-2}$ as a result of constraint in the development of a large plastic zone in the resin-rich region between plies due to the fibres in the adjacent plies [13, 32].

4.3. Mode II interlaminar fracture toughness

With regard to the Mode II toughness data (Table I and Fig. 10), it can be seen that at low bead volume fractions an increase in toughness is obtained, while at high volume fractions there is a fairly dramatic drop-off. The fall-off is believed to be a consequence of a relatively thick bead-filled interlayer being present at high bead contents which fails in shear relatively easily because it is not constrained effectively by the fibres. The Mode II interlaminar fracture toughness values are high compared to the Mode I interlaminar fracture toughness as found by many other workers studying moderate- and low-toughness systems [31, 32]. This is associated with the failure mechanism in the Mode II test, namely the formation of sigmoidal shaped microcracks over a considerable distance ahead of the crack tip, causing significant load redistribution.

In Table I it is shown that the ratio of Mode II to I fracture toughness (G_{IIC}/G_{IC}), decreases with increasing bead volume fraction. It has been reported that the ratio of G_{IIC} to G_{IC} of brittle matrix composites is generally higher than that of ductile matrix composites and that the ratio (G_{IIC}/G_{IC}) of very tough matrix composites approaches unity [13, 31, 32]. The data of Table I follow this general trend; they show a reducing G_{IIC}/G_{IC} ratio with increasing beads consistent with tougher behaviour.

Scanning electron micrographs of the fracture surfaces of ENF specimens are shown in Fig. 12. Compared with the DCB specimens (Fig. 11), there is little fibre bridging in the ENF specimens. In the unmodified epoxy glass-fibre composite and at low bead volume fractions (Fig. 12a), many uneven looking facets (or hackles) can be seen. These arise during crack growth from the formation of the sigmoidal shaped matrix microcracks ahead of the crack tip with an orientation of approximately 45° to the fibre direction (which for Mode II loading is the principal tensile stress plane) [17, 35]. By contrast, Mode I failure occurs with the development of a small deformation zone ahead of the crack tip. The occurrence of hackles in Mode II loading decreases with increasing bead volume fraction in the matrix, as shown in Fig. 12. This is most marked at the highest bead fraction, where not only are few hackles visible but also the number of bare debonded fibres seen in the fracture surface of the 20% hybrid composite is reduced compared to the other materials. These effects arise presumably from the presence of the relatively thick bead-filled interlayer at this high bead volume fraction. It is likely that the thick interlayer fails in shear comparatively easily, because it is not constrained effectively by the fibre and hence the sigmoidal shaped hackles are not formed.

5. Conclusion

Based on the results of fracture toughness evaluation of carbon and phenolic bead-filled epoxies, six different composites (pure epoxy glass-fibre composite, 10%, 15%, 20%, 30% by volume of matrix carbon bead-reinforced hybrid composite and a 15% by volume of matrix phenolic bead-reinforced hybrid composite) were fabricated. The interlaminar fracture toughness of these hybrid composites was evaluated to investigate interlaminar fracture behaviour. Optimum bead volume fraction for enhancing the interlaminar fracture toughness was also discussed.

The pure epoxy glass-fibre composite showed the greatest R-curve behaviour due to the large amount of fibre bridging resulting from the filament winding method of laminate fabrication. The carbon bead-reinforced hybrid composite material showed an increase in Mode I interlaminar toughness at crack-growth initiation, compared to the standard epoxy laminate. The optimum bead volume fraction for G_{IC} and K_{IC} initiation values is between 15% and 20% (the 15% and 20% hybrid composites showed the highest K_{IC} and G_{IC} initiation values, respectively). The carbon bead-reinforced hybrid composites showed higher toughness than the phenolic bead-reinforced hybrid composites at the same volume fraction (15%). This suggests that transparticle fracture and associated crack-tip blunting is more effective than crack pinning in the improvement of the interlaminar toughness of hybrid composites.

The Mode II interlaminar fracture toughness of ENF specimens (machined from the same composite panels as the DCB specimens) shows high toughness compared to the Mode I interlaminar fracture toughness. This is believed to be due to a different fracture mechanism related to the formation of sigmoidal shaped microcracks as evinced by hackles in the fracture surface. Carbon bead-reinforced hybrid composites show an optimum Mode II interlaminar fracture toughness at a bead volume fraction of about 15%. However, at a higher bead volume fraction (20%) a sharp drop occurs. This is suggested to be a consequence of a different fracture mechanism occurring within a thicker bead-filled interlayer.

References

1. C. Y. KAM and J. V. WALKER, in "Toughened composite", edited by N. J. Johnston, ASTM STP 937 (American Society for Testing and Material, Philadelphia, PA, 1987) p. 9.
2. P. K. MALLIC and S. NEWMAN, "Composite Materials Technology" (Hanser, Munich, Vienna, New York, 1990) Ch. 1, p. 10.
3. R. C. TENNYSON, in "Proceedings of the International Conference on Composite Engineering (ICCE/I)", edited by David Hui (ICCE, New Orleans, 1994) p. 11
4. W. M. JORDAN and W. L. BRADLEY, in "Toughened composite", edited by N. J. Johnston, ASTM STP 937 (American Society for Testing and Material, Philadelphia, PA, 1987) p. 95
5. B. Z. JANG, J. Y. LIAU, L. R. HWANG and W. K. SHIH, *J. Reinf. Plast. Compos.* **8** (1989) 312.
6. J. KIM, C. BAILLIE, J. POH and Y. W. MAI, *Compos. Sci. Technol.* **43** (1992) 283.
7. D. HULL, *J. Mater. Sci. Eng.* **A184** (1994) 173.
8. F. N. COGSWELL and M. HOPPER, *Composites* **3** (1983) 251.
9. F. N. COGSWELL and D. C. LEACH, *Plast. Rubber Proc. Applic.* **4** (1984) 271.
10. A. C. GARG and Y. W. MAI, *Compos. Sci. Technol.* **37** (1988) 179.
11. F. N. COGSWELL, "Thermoplastic aromatic polymer composites" (Butterworth-Heinemann, Oxford, 1992) Ch. 3, p. 51.
12. W. D. BASCOM, R. Y. TING, R. J. MOULTON and A. R. SIEBERT, *J. Mater. Sci.* **16** (1981) 2657.

13. W. L. BRADLEY, *Key Eng. Mater.* **37** (1989) 101.
14. R. E. EVANS and J. E. MASTER, in "Toughened composite", edited by N. J. Johnston, ASTM STP 937 (American Society for Testing and Material, Philadelphia, PA, 1987) p. 413.
15. F. F. LANGE, *Philos. Mag.* **22** (1970) 983.
16. J. S. SPANOUDAKIS and R. J. YOUNG, *J. Mater. Sci.* **19** (1984) 473.
17. A. C. MOLONEY, H. H. KAUSCH and H. R. STIEGER, *ibid.* **18** (1983) 208.
18. A. C. MOLONEY, H. H. KARSCH, T. KAISER and H. R. BEER, *ibid.* **22** (1987) 381.
19. B. Z. JANG, J. Y. LIAU, L. R. HWANG and W. K. SHIH, *J. Reinf. Plast. Compos.* **9** (1990) 314.
20. J. K. KIM and P. E. ROBERTSON, *J. Mater. Sci.* **27** (1992) 161.
21. C. DORAN, S. L. OGIN and P. A. SMITH, in "Advanced Composites in Emerging Technologies", edited by S. A. Paipetis and T. P. Philippidis (AMATEC, Patras, Greece, 1991) p. 181.
22. Manufacturer's technical data, "Spherical carbon powder" (1989).
23. J. J. LEE, S. L. OGIN and P. A. SMITH, "Proceedings of the 5th PRI International Conference on Fibre Reinforced Composites", FRC '92, University of Newcastle upon Tyne, 24–26 March 1992 p. 22/1.
24. J. J. LEE, Ph D thesis, University of Surrey (1992).
25. "Protocols for Interlaminar Fracture Testing of Composites", edited by P. Davies, European Structural Integrity Society Polymers and Composite Task Group, March (1992 revision).
26. R. M. L. FOOTE and V. T. BUCHWALD, *Int. J. Fract.* **29** (1985) 125.
27. J. K. KIM, C. A. BAILLIE, J. POH and Y. M. MAI, *Compos. Sci. Technol.* **43** (1992) 283.
28. G. M. NEWAS, *Eng. Frac. Mech.* **29** (1988) 31.
29. A. J. RUSSEL and K. N. STREET, in "Delamination and debonding of materials", edited by W. S. Johnston, ASTM STP 876 (American Society for Testing and Material, Philadelphia, PA, 1985) p. 349.
30. S. HASHEMI, A. J. KINLOCH and J. G. WILLIAMS, *Compos. Sci. Technol.* **37** (1990) 429.
31. M. F. HIPPS, M. K. TSE and W. L. BRADLEY, in "Toughened composite", edited by N. J. Johnston, ASTM STP 937 (American Society for Testing and Materials, Philadelphia, PA, 1989) p. 115.
32. W. L. BRADLEY, in "Application of fracture mechanics to composite materials", Composite material series, edited by K. Friedrich, (Elsevier Science, 1989) p. 159.
33. A. J. KINLOCH, S. J. SHAW and D. A. TOD, *Polymer* **24** (1983) 1341.
34. D. L. HUNSTON and R. DEHL, "The role of polymer toughness in matrix dominated composite fracture", paper EM87-355 (Society of Manufacturing Engineers, Dearbon, MI, 1987).
35. H. J. SUE, R. E. JONES and E. I. GARCIA-MEITIN, *J. Mater. Sci.* **28** (1993) 6381.

Received 17 February
and accepted 24 May 1995